





## Article

# Corrosion Resistance of Titanium Alloys Anodized in Alkaline Solutions

Facundo Almeraya-Calderón <sup>1</sup>, Jesús M. Jáquez-Muñoz <sup>1,2,\*</sup>, Erick Maldonado-Bandala <sup>3</sup>,  
Jose Cabral-Miramontes <sup>1</sup>, Demetrio Nieves-Mendoza <sup>3</sup>, Javier Olgui-Coca <sup>4</sup>, Luis Daimir Lopez-Leon <sup>4,\*</sup>,  
Francisco Estupiñán-López <sup>1</sup>, Alejandro Lira-Martínez <sup>2</sup> and Citlalli Gaona Tiburcio <sup>1</sup>

<sup>1</sup> Centro de Investigación e Innovación en Ingeniería Aeronáutica (CIIIA), Universidad Autónoma de Nuevo León, FIME, San Nicolás de los Garza 66455, Mexico; facundo.almerayacl@uanl.edu.mx (F.A.-C.); jose.cabralmr@uanl.edu.mx (J.C.-M.); francisco.estupinanlp@uanl.edu.mx (F.E.-L.); citlalli.gaonatbr@uanl.edu.mx (C.G.T.)

<sup>2</sup> Facultad de Ingeniería, Universidad Autónoma de Ciudad Juárez, Ciudad Juárez Chihuahua 32320, Mexico; manuel.lira@uacj.mx

<sup>3</sup> Facultad de Ingeniería Civil/Facultad de Arquitectura, Universidad Veracruzana, Xalapa 91000, Mexico; erimaldonado@uv.mx (E.M.-B.); dneives@uv.mx (D.N.-M.)

<sup>4</sup> Área Académica de Ingeniería y Arquitectura, Universidad Autónoma del Estado de Hidalgo, Carretera Pachuca-Tulancingo, Km 4.5, Hidalgo 42082, Mexico; olguinc@uaeh.edu.mx

\* Correspondence: jesus.jaquezmn@uanl.edu.mx (J.M.J.-M.); luis\_lopez@uaeh.edu.mx (L.D.L.-L.)

**Abstract:** Titanium alloys present superior electrochemical properties due to the generation of the TiO<sub>2</sub> passive layer. The ability to generate an oxide passive layer depends on the anodized alloy. This work mainly studies the corrosion resistance of the alloys Ti-6Al-2Sn-4Zr-2Mo and Ti-6Al-4V anodized in NaOH and KOH at 1 M and 0.025 A/cm<sup>2</sup> of current density. The electrochemical techniques were performed in a conventional three-electrode cell exposed to electrolytes of NaCl and H<sub>2</sub>SO<sub>4</sub>. Based on ASTM-G61 and G199, cyclic potentiodynamic polarization (CPP) and electrochemical noise (EN) techniques were used. The results indicated that Ti-6Al-2Sn-4Zr-2Mo anodized on NaOH presented a higher passivity range than anodized on KOH, relating to the high reactivity of Na<sup>+</sup> ions. The former anodized alloy also demonstrated a higher passive layer rupture potential. In EN, the results showed that Ti-6Al-4V anodized in KOH presented a trend toward a localized process due to the heterogeneity of anodized porosity and the presence of V in the alloy.

**Keywords:** titanium; anodized; electrochemical noise; wavelets; potentiodynamic polarization



**Citation:** Almeraya-Calderón, F.; Jáquez-Muñoz, J.M.; Maldonado-Bandala, E.; Cabral-Miramontes, J.; Nieves-Mendoza, D.; Olgui-Coca, J.; Lopez-Leon, L.D.; Estupiñán-López, F.; Lira-Martínez, A.; Gaona Tiburcio, C. Corrosion Resistance of Titanium Alloys Anodized in Alkaline Solutions. *Metals* **2023**, *13*, 1510. <https://doi.org/10.3390/met13091510>

Academic Editors: Fahe Cao and Branimir N. Grgur

Received: 19 July 2023

Revised: 16 August 2023

Accepted: 21 August 2023

Published: 23 August 2023



**Copyright:** © 2023 by the authors. Licensee MDPI, Basel, Switzerland. This article is an open access article distributed under the terms and conditions of the Creative Commons Attribution (CC BY) license (<https://creativecommons.org/licenses/by/4.0/>).

## 1. Introduction

Titanium and its alloys have been employed in many industries due to their corrosion resistance, and the same industries boost the study of the oxide layer of Ti alloys. The aerospace industry employs significant quantities of Ti-alloys due to the demanding performance of components and the requirement for a high working life of the components [1–4]. The analysis of oxide layers on Ti-alloys has increased because of their excellent chemical and biological properties [1]. The use of titanium over other alloys (steel and superalloys) is due to its low density; factors such as fatigue resistance and the electrochemical compatibility of titanium and carbon fiber are essential parameters to use in the aerospace industry [5].

The principal applications of Ti alloys in the aerospace industry are for crucial zones such as window frames, landing gear, clips, wing sections (ribs), brackets, and compressor areas. The principal alloys employed for those applications are Ti-6Al-2Sn-4Zr-2Mo and Ti-6Al-4V [6–10].

The titanium generates an oxide layer that passivates the material and makes it more resistant to corrosion. However, the natural passive layer created on Ti is susceptible to Cl<sup>−</sup> attacks due to the heterogeneities of the oxide layer. OH<sup>−</sup> and Cl<sup>−</sup> ions in the electrolytes

generate attacks by interstitial penetration in the oxide layer [11,12]. Therefore, the authors suggest different methods to increase corrosion resistance, such as passivation, the addition of alloy elements, or anodizing. The oxide layer generated by passivation is usually amorphous [13–15]. The authors reported that the passive layer is homogenous when passivate is generated in pure titanium (Ti CP2 or any CP). However, when the passivation is created in titanium alloy, the passive layer can be heterogeneous due to the difference in alloying elements; adding a small oxide layer can be a problem due to the penetration of different ions ( $\text{Cl}^-$ ,  $\text{OH}^-$  or  $\text{SO}_4^{2-}$ ) in the surface by interstitial mechanisms [16–20]. Other options to protect titanium are plasma electrolytic oxidation (PEO) and sol-gel coatings; those techniques require special equipment to generate the layer, and the cost and difficulty of coating increase in some geometries [21,22].

Considering the disadvantages of the past methods, an excellent option to generate a passive layer is the anodizing process; the influence of current or potential helps to develop a uniform layer, increasing the thickness and creating a more homogenous morphology. The anodization forms insoluble oxide layers on a metal surface using potential and/or current to generate the oxide layer. Usually, the growth of oxide is related to the current. After some time, the current can dissolve the oxide layer at specific points, beginning with the pores [23]. Factors such as pH, temperature, and time can control the formation of anodized aluminum [24].

Diverse works suggest the application of fluoride to generate better passive layers on the Ti surface; however, using fluoride acid has several problems, such as the difficulty of solution management, and modern authors keep looking for options to generate the oxide layer [25]. When titanium is anodized in a basic or acidic solution, the  $\text{TiO}_2$  passive layer is created at a potential lower than the breakdown potential. Usually, anodized surfaces present colors due to the high dielectric constant of the  $\text{TiO}_2$  barrier [26]. Some options for fluoride electrolytes are  $\text{KNO}_3$ ,  $\text{H}_3\text{PO}_4$ ,  $\text{H}_2\text{SO}_4$ ,  $\text{NaOH}$ ,  $\text{NaNO}_3$ , etc. [11].

Other factors, such as potential, are related to the crystalline structure; high potentials have a crystalline structure, and low potentials present amorphous structures. If anodizing time increases, the formation of a crystalline structure is more probable. The titanium anodizing mechanism forms an oxide layer (continuous without porosity). After the oxide layer's formation, pitting is caused by ions ( $\text{OH}^-$ ,  $\text{SO}_4^{2-}$ ,  $\text{PO}_4^{3-}$ , e.g.). The increase in potential anodization is related to an increased resistance to corrosion of the anodic layer [27,28].

Nakajima et al. [29] mentioned that the anodized process is complex, involving film growth, film breakdown, current, potential, temperature, and pH. Therefore, the process is not completely understood, and it is necessary to investigate more about the theme. The results showed that the anodized material obtained presented high porosity; however, Ti-6Al-4V presented better properties than those obtained in the  $\beta$  alloy. They conclude that the chemical composition of the alloy has a high importance in the formation of the anodized coating; in that case, when  $\beta$  stabilizers increase, the properties of the coating against corrosion decrease when anodized in basic media.

Authors such as Acevedo-Peña [30] reported high corrosion resistance when  $\text{TiO}_2$  is higher in the coating. Suboxides such as  $\text{TiO}$  and  $\text{Ti}_2\text{O}_3$  showed less protection against corrosion. The oxide layer's degradation was related to the hydroxyl transport in the vacancies. The Ti-alloys exposed in alkaline media presented a passivation zone when studied by potentiodynamic polarization, indicating that alloys tend to form a natural passive layer [31].

Electrochemical techniques are a powerful option to characterize properties such as corrosion resistance, porosity, and the type of reaction occurring on the material surface. Different authors used potentiodynamic polarization to determine corrosion resistance, and results showed a decrease in  $i_{\text{corr}}$ , relating the result to the reduction in corrosion rate [32].

Prando et al. anodized titanium and found that in the presence of chloride ions, localized corrosion is caused by the migration of ions across the passive film due to the accumulation of oxychloride at the metal-oxide interface, provoking the rupture of the

passive layer [33]. In past research on anodizing in acid media, Ti-6Al-2Sn-4Zr-2Mo presented better properties against corrosion. Meanwhile, Ti-6Al-4V showed lower corrosion resistance. The electrochemical noise technique of wavelets analysis predicted porosity, and Ti-6Al-4V presented the most heterogeneous porosity when high accumulation energy appeared on the first wavelets crystals [34,35].

Considering an industrial environment, sulfuric acid can simulate an environment of acid rain. It is formed from the chemical reactions of sulfur dioxide and nitrogen oxides found in the atmosphere with water and chemical contaminants, resulting in nitric sulfuric acids. This work aimed to study the corrosion resistance of the alloys Ti-6Al-2Sn-4Zr-2Mo and Ti-6Al-4V anodized in NaOH and KOH at 1 M, employing the techniques of cyclic potentiodynamic polarization (CPP) and electrochemical noise (EN). The electrolytes used were NaCl and H<sub>2</sub>SO<sub>4</sub> solutions at 3.5 wt.% as a simulation of marine and industrial atmospheres. Titanium alloys used in various components in aircraft are exposed to different atmospheres, such as marine and industrial (acid rain). Exposure to marine environments has the presence of chlorides as a corrosive agent.

## 2. Materials and Methods

### 2.1. Materials

The materials employed were commercial (Supra Alloys, Camarillo, CA, USA) titanium alloys (AMS Aerospace Material Specifications): Ti-6Al-2Sn-4Zr-2Mo (AMS 4917) and Ti-6Al-4V (AMS 4911), obtained in a cylindrical extruded bar with a diameter of 2 in and a length of 12 in. The chemical composition of these Ti-alloys was obtained by X-ray fluorescence. Table 1 shows the chemical composition of each alloy.

**Table 1.** Chemical composition of the Ti-6Al-2Sn-4Zr-2Mo (AMS 4917) and Ti-6Al-4V (AMS 4911) alloys (wt.%).

Elements	Ti-6Al-2Sn-4Zr-2Mo AMS 4917	Ti-6Al-4V AMS 4911
Ti	84.65 ± 0.19	87.71 ± 0.36
Al	6.75 ± 0.20	7.14 ± 0.37
Sn	2.08 ± 0.01	–
V	–	4.03 ± 0.08
Zr	4.18 ± 0.01	–
Mo	1.99 ± 0.008	–

### 2.2. Anodized Process

Pretreatment consisted of ultrasonic cleaning in ethanol and deionized water. The anodizing process was carried out in the electrolytes of NaOH and KOH at 1 M concentration at 25 °C ± 1 [analytical grade reagents (JT Baker, Phillipsburg, NJ, USA)], in an electrochemical cell with a platinum mesh as the cathode. The current density of the titanium samples was 0.025 A/cm<sup>2</sup> for 600 s using a DC power supply (XLN300025-GL). The anodizing process was carried out under the specification AMS2487 [36].

### 2.3. Microstructural Characterization

Titanium alloys were prepared by metallography. The materials were polished using various SiC sandpaper grades 400–800; each sample was ultrasonically cleaned for 10 min in ethanol and deionized water. The samples were subjected to a chemical attack using a Kroll solution.

The surface section of titanium alloys was investigated using secondary electron (SE) detectors in a scanning electron microscope (SEM, JEOL-JSM-5610LV, Tokyo, Japan) operating at 20 kV and 8.5 and 12 mm work distances.

#### 2.4. Electrochemical Measurements

The CPP and EN measurements were conducted at room temperature using a Gill-AC potentiostat/galvanostat/ZRA (Zero Resistance Ammeter) from ACM Instruments (Cumbria, UK) in 3.5 wt.% NaCl and H<sub>2</sub>SO<sub>4</sub> solutions. A conventional three-electrode cell was used for electrochemical corrosion studies. The anodized samples were the working electrode, WE (1 cm<sup>2</sup>), the reference electrode, RE (saturated calomel electrode, SCE), and the counter electrode, CE (platinum mesh). Corrosion tests were realized in triplicate.

The CPP measurement parameters ranged from −1.2 to 1.2 V vs. the SCE of the corrosion potential ( $E_{\text{corr}}$ ). A complete polarization cycle was used at 1 mV/s [37,38].

The EN technique was studied at 1 data point per second; the time records comprised 4096 data points. The EN signal was processed with MATLAB 2018a to obtain the fast Fourier transform and wavelet analysis [39].

### 3. Results

#### 3.1. SEM Superficial Analysis

Figure 1 shows the different superficial morphologies of the anodized samples. The morphology of Ti-6Al-2Sn-4Zr-2Mo anodized in NaOH (Figure 1a) showed that the surface presented different roughness due to the difference in the height of the anodized, indicating that it is not homogenous; this anodized presented cracks in the surface. Figure 1b of Ti-6Al-4V anodized in NaOH presented a similar morphology, which is attributed to the difference in phase in Ti-alloys. The anodized process was performed selectively in the  $\alpha$  phase; meanwhile, the  $\beta$  phase presented more difficulty generating an oxide layer.

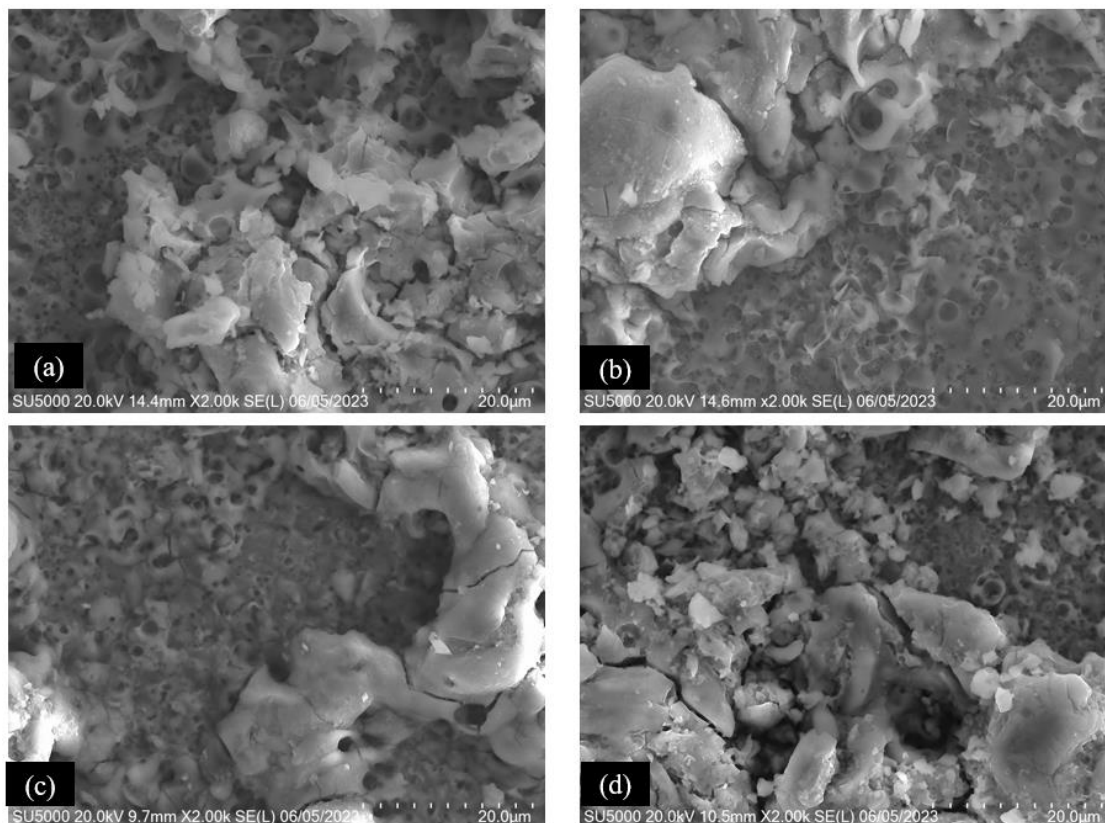


**Figure 1.** SEM-SE Micrograph of (a) Ti-6Al-2Sn-4Zr-2Mo anodized in NaOH; (b) Ti-6Al-2Sn-4Zr-2Mo anodized in KOH; (c) Ti-6Al-4V anodized in NaOH; and (d) Ti-6Al-4V anodized in KOH.

Figure 1c shows the morphology of Ti-6Al-2Sn-4Zr-Mo anodized in KOH, and this anodized material presented a heterogeneous layer with different altitudes. The behavior of that morphology is related to the difference in the phase of the alloy. The Ti-6Al-4V



anodized in KOH shown in Figure 1d presented a similar morphology to the Ti-6Al-2Sn-4Zr-2Mo anodized in KOH. The only difference is that the anodized Ti-6Al-4V presented more cracks. Both anodized electrolytes developed a heterogeneous oxide layer with cracks in the surface and porosities.

The anodized Ti-6Al-4V presented a more heterogeneous surface than Ti-6Al-2Sn-4Zr-2Mo due to a higher presence of  $\beta$  stabilizer, V, and Mo, respectively. Authors have reported that Ti-alloys with a V presence present more difficulty in generating a homogenous oxide layer and facilitate the corrosion process.

### 3.2. Cyclic Potentiodynamic Polarization

The corrosion kinetic behavior using CPP can be observed through cathodic and anodic reactions in polarization curves to obtain the electrochemical parameters (corrosion current density,  $i_{\text{corr}}$ ; passivation current density,  $i_{\text{pass}}$ ; potential corrosion,  $E_{\text{corr}}$ ; and pitting potential,  $E_{\text{pit}}$ ).

Figure 2 shows the CPP results for both media exposed to NaCl. The Ti-6Al-4V anodized in KOH showed a current density of  $1.06 \times 10^{-7} \text{ A/cm}^2$ , being the lowest, relating the result to a lower corrosion kinetic. On the other hand, the same alloy anodized in NaOH presented a higher corrosion kinetic with an  $i_{\text{corr}}$  of  $3.20 \times 10^{-6} \text{ A/cm}^2$ , meaning a higher corrosion kinetic when exposed to NaCl. That behavior is related to easy ion penetration in the anodized surface due to a non-homogenous surface; this occurs due to an accumulation of  $\text{Cl}^-$  in the form of oxychloride that penetrates the oxide layer [40].

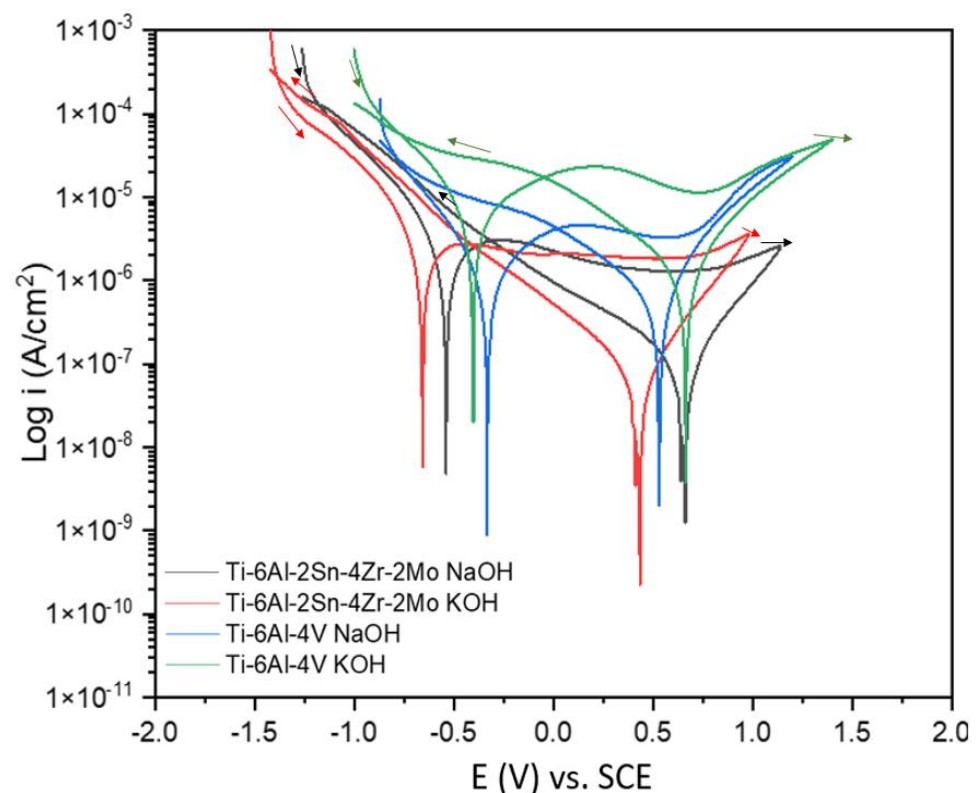


**Figure 2.** CPP for Ti-6Al-2Sn-4Zr-2Mo and Ti-6Al-4V alloys anodized and exposed in a 3.5 wt.% NaCl solution.

Analyzing the passivation range (see Table 1), the alloy Ti-6Al-2Sn-4Zr-2Mo presented the most extended passivation range in both anodized electrolytes when exposed to NaCl. The anodized NaOH showed 1.27 V, and in KOH, 1.25 V. Thus, the species accumulation domain was on the anodized surface. Different authors associated the high corrosion resistance of Ti-alloys with the presence of Zr and Mo. Those elements' presence helps create an oxide layer with better properties against corrosion [41,42]. For that reason, the

dissolution of anodized aluminum is reduced, and even the oxide layer can increase due to the difficulty of ion penetration.

One crucial factor is the passivation current; in this case, Ti-6Al-4V anodized in KOH presented the highest value of  $\times 10^{-5}$  order; meanwhile, the rest of the alloys showed values of  $\times 10^{-6}$  A/cm<sup>2</sup>, meaning that the anodized Ti-6Al-4V in KOH will present a higher dissolution. Furthermore, that result is related to  $i_{\text{corr}}$ , so the corrosion kinetics of anodized will be faster. The passive layer breakdown potential is lower for Ti-6Al-4V anodized in NaOH (0.61 V vs. SCE). It is essential to mention that Ti-6Al-4V presented this potential in the middle of the passivation process, presenting a higher slope to an increase in current density. This behavior can be related to the instability of an anodized surface due to the heterogeneity of anodized porous materials. The increase in corrosion kinetics of Ti-6Al-4V anodized is associated with V presence, which reduces the corrosion resistance of the oxide layer; the V makes the anodized prone to interstitial ion attacks [43,44].

All the samples presented negative hysteresis due to the uniform corrosion process. Moreover, currents in the back curve are lower and potentials are higher; that result is associated with protecting the uniform process relating to species diffusion [45]. The unstable use of Na<sup>+</sup> reduces the effectiveness of TiO<sub>2</sub>. Furthermore, the authors showed that titanium is susceptible to crevice corrosion in NaCl, and that behavior can be related to localized processes [46].

The increase in  $E_{\text{corr}}$  in the different anodized samples is related to an increase in corrosion resistance due to the formation of a composite layer; however, the  $i_{\text{corr}}$  increases when  $E_{\text{corr}}$  increases, so the meaning is related to the necessity of more energy to begin with in the anodic process [47–49].

Figure 3 shows the CPP results when anodizing samples were exposed to H<sub>2</sub>SO<sub>4</sub> at 3.5 wt.%. The samples of Ti-6Al-4V anodized in both electrolytes presented a higher corrosion density, with values of  $4.66 \times 10^{-6}$  and  $9.65 \times 10^{-6}$  A/cm<sup>2</sup>; this value means that this alloy presented the anodized with less corrosion resistance. The relationship with V is shown in this environment, indicating that V facilitates the corrosion process in the anodize.

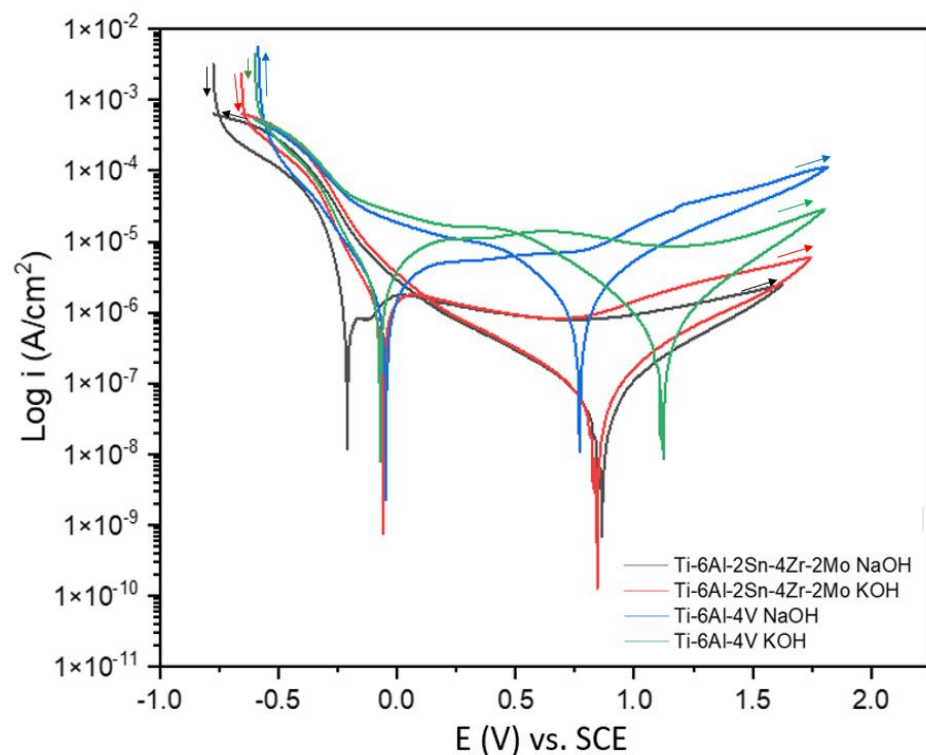


**Figure 3.** CPP for Ti-6Al-2Sn-4Zr-2Mo and Ti-6Al-4V alloys anodized and exposed in a 3.5 wt.% H<sub>2</sub>SO<sub>4</sub> solution.

On the other hand, the anodizes of the alloy Ti-6Al-Sn-4Zr-2Mo presented a better behavior against anodized dissolution. The behavior of the passivation range shows that Ti-6Al-4V also has lower values (0.63 and 0.44 V). It can be associated with a heterogeneous surface, and its auspices govern the reactions in those zones. A critical relation was shown in the potential of the breakdown of the passive layer, where anodized samples in KOH presented the lower values, 0.72 and 0.63 V for Ti-6Al-2Sn-4Zr-2Mo and Ti-6Al-4V, respectively. That result is related to a heterogeneous process in which the electrolyte anodizes. Ti-6Al-4V showed a higher  $i_{\text{pass}}$ , associated with a fast kinetic in the dissolution of the layer created on an anodized surface.

Meanwhile, Ti-6Al-2Sn-4Zr-2Mo anodized in NaOH presented a lower value ( $\times 10^{-7}$  A/cm<sup>2</sup>). It is related to lower electrons' transference and a more stable layer. All results of the CPP indicate a higher corrosion resistance in his sample. All the samples presented negative hysteresis relating to the uniform process. Some authors agree with the theory that the heterogenous surface (pores and surface cracks) makes it easy for the electrolyte to attack the metal surface, passing the coating [50,51]. Liu et al. [52] mentioned that the corrosion mechanism of this electrolyte in titanium coatings acts in four stages. Penetration causes a change in potential. The next stage is stabilization when the electrolyte is added, and under the auspices of the three stages are coating dissolution and, finally, the localized attack of the material surface. In this research, a localized attack was not found. The results can be associated with stage 1 of the process, when ion penetration causes the breaking of the passive layer created on the surface. This behavior is related to the one presented by Fekry [53], who concluded that the  $\text{SO}_4^{2-}$  and  $\text{Cl}^-$ , where the corrosion products were soluble, dissolved the oxide layer created in the anodic breach.

Authors have reported that in the cathodic layer occurs a hydrogen evolution; that behavior can sensitize the anodized and provoke a faster anodization dissolution, as is shown for the anodization of Ti-6Al-4V in NaOH. The Ti-6Al-4V anodized in KOH showed regeneration of the passive layer, but a dissolution process occurred, so the passive layer generated is not protective enough [54].

The shape of the CPP curve Figures 2 and 3 of the titanium alloys have similar behavior; the anodic reaction begins in activation, followed by passivation, with pitting potential and negative hysteresis, which indicates uniform corrosion.

Table 2 shows the parameters obtained by CPP. Anodized Ti-6Al-4V presented properties with a higher trend toward dissolution. In addition, samples anodized in KOH showed lower corrosion resistance as a heterogeneous surface.

**Table 2.** Parameters obtained by CPP for Ti-6Al-2Sn-4Zr-2Mo and Ti-6Al-4V alloys anodized.

Alloys	Anodizing Electrolyte	$E_{\text{corr}}$ (V)	$i_{\text{corr}}$ (A/cm <sup>2</sup> )	$E_{\text{pit}}$ (V)	$R_{\text{pass}}$ (V)	$i_{\text{pass}}$ (A/cm <sup>2</sup> )	Hysteresis
Immersed in 3.5 wt.% NaCl Solution							
Ti-6Al-2Sn-4Zr-2Mo	NaOH	−0.52	$6.98 \times 10^{-7}$	0.83	1.27	$3.03 \times 10^{-6}$	negative
Ti-6Al-2Sn-4Zr-2Mo	KOH	−0.64	$5.55 \times 10^{-7}$	0.73	1.25	$2.58 \times 10^{-6}$	negative
Ti-6Al-4V	NaOH	−0.32	$1.06 \times 10^{-7}$	0.61	0.55	$4.33 \times 10^{-6}$	negative
Ti-6Al-4V	KOH	−0.40	$3.20 \times 10^{-6}$	0.77	0.59	$2.28 \times 10^{-5}$	negative
Immersed in 3.5 wt.% H <sub>2</sub> SO <sub>4</sub> Solution							
Ti-6Al-2Sn-4Zr-2Mo	NaOH	−0.19	$5.51 \times 10^{-7}$	1.01	0.82	$1.67 \times 10^{-7}$	negative
Ti-6Al-2Sn-4Zr-2Mo	KOH	−0.05	$7.53 \times 10^{-7}$	0.72	0.69	$1.75 \times 10^{-6}$	negative
Ti-6Al-4V	NaOH	−0.05	$1.05 \times 10^{-6}$	0.83	0.63	$4.66 \times 10^{-6}$	negative
Ti-6Al-4V	KOH	−0.05	$2.26 \times 10^{-6}$	0.63	0.44	$9.65 \times 10^{-6}$	negative

### 3.3. Electrochemical Noise

#### 3.3.1. Power Spectral Density (PSD) and Noise Impedance (Zn)

The EN signal was filtered by a polynomial method employing a 9th-grade (Eden and Rothwell, 1992; Cottis and Turgoose, 1999) [55,56] by Equation (1):

$$y_n = x_n - \sum_{i=0}^{p_0} a_i n^i \quad (1)$$

The PSD was calculated employing a fast Fourier transform (FFT) based on Equation (2) [57].

$$\Psi_x(k) = \frac{\gamma \cdot t_m}{N} \cdot \sum_{n=1}^N (x_n - \bar{x}_n) \cdot e^{-\frac{2\pi k n^2}{N}} \quad (2)$$

Figure 4 shows the PSD for the current signal of anodized exposure in NaCl (a) and H<sub>2</sub>SO<sub>4</sub>. For Figure 4a, all samples presented slope values from  $-7$  to  $-9$  (see Table 3). It is related to localized reactions or preferential zones due to a high and probably heterogeneous porosity. In addition, all the anodize showed changes in the slope in the frequency range, indicating that different processes occur on the surface due to the heterogeneity of this one. The Ti-6Al-4V anodized in KOH presented the higher  $\psi^0$  value, with  $-118$  dBi, indicating that corrosion kinetics occur faster for this alloy in this environment.

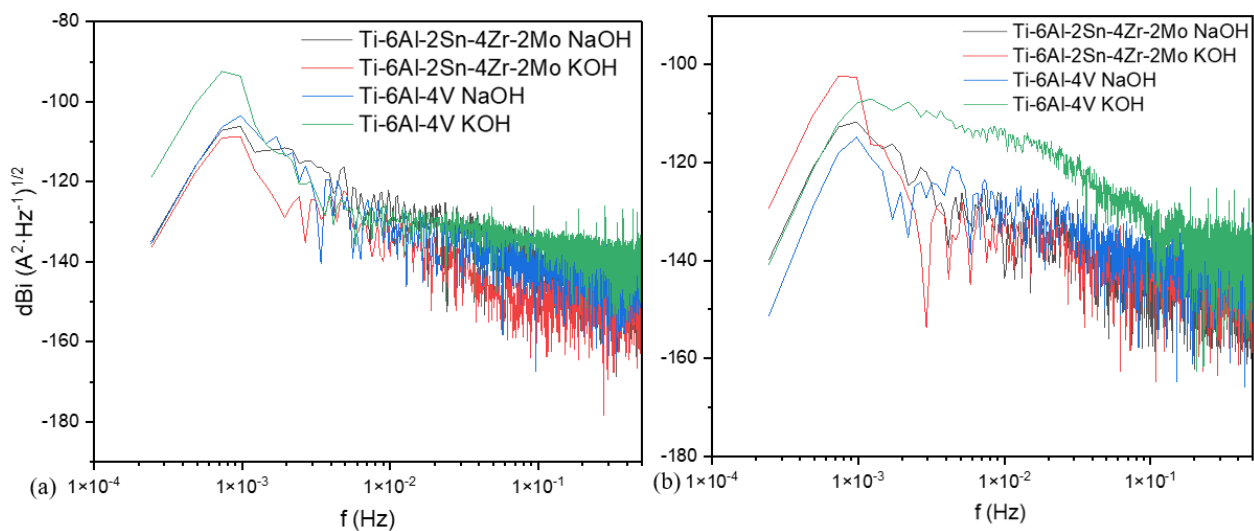


**Figure 4.** PSD in current of Ti-6Al-2Sn-4Zr-2Mo and Ti-6Al-4V, alloys anodized and immersed in (a) NaCl and (b) H<sub>2</sub>SO<sub>4</sub> at 3.5 wt.%.

**Table 3.** Noise Impedance ( $Z_n$ ) and  $\Psi^0$  for Ti-6Al-2Sn-4Zr-2Mo and Ti-6Al-4V alloys anodized and immersed in 3.5 wt.% NaCl and H<sub>2</sub>SO<sub>4</sub>.

Alloys	Anodizing Electrolyte	$\Psi^0$ (dBi)	B (dB [A])	$Z_{n0}$ ( $\Omega \cdot \text{cm}^2$ )
Immersed in 3.5 wt.% NaCl Solution				
Ti-6Al-2Sn-4Zr-2Mo	NaOH	$-134$	$-9.9$	$87.80 \times 10^4$
Ti-6Al-2Sn-4Zr-2Mo	KOH	$-136$	$-7.3$	$12.46 \times 10^3$
Ti-6Al-4V	NaOH	$-135$	$-7.2$	$72.53 \times 10^3$
Ti-6Al-4V	KOH	$-118$	$-7.9$	$29.57 \times 10^3$
Immersed in 3.5 wt.% H <sub>2</sub> SO <sub>4</sub> Solution				
Ti-6Al-2Sn-4Zr-2Mo	NaOH	$-139$	$-6.3$	$16.75 \times 10^3$
Ti-6Al-2Sn-4Zr-2Mo	KOH	$-129$	$-5.3$	$1.48 \times 10^3$
Ti-6Al-4V	NaOH	$-151$	$-4.5$	$18.66 \times 10^4$
Ti-6Al-4V	KOH	$-140$	$-12.7$	$19.75 \times 10^3$



For samples in  $H_2SO_4$ , only Ti-6Al-4V presented a slope related to the localized process; the others presented a uniform process. Wei et al. [58] conclude that titanium tends to form an excellent  $TiO_2$  coating (adherence, strength, and inertness), but the oxide layer created has low valence. In the presence of strong acid, it will dissolve the oxide layer. In this medium, the anodized KOH presented higher  $\psi^0$  values, showing a high corrosion kinetic for anodized in that electrolyte. That behavior is related to the role of  $Na^+$  ions, making the anodization process easy [59,60].

Figure 5 shows the noise impedance ( $Z_n$ ) of anodized aluminum exposed to NaCl (a) and  $H_2SO_4$ . The slope behavior is similar to PSD, where Ti-6Al-4V presented a change in slope due to the different processes that occur on surfaces. In Figure 5a, sample Ti-6Al-2Sn-4Zr-2Mo presented a higher  $Z_n$  of  $87.8 \times 10^4 \Omega \cdot cm^2$ . Meanwhile, both anodized in KOH presented  $12.43 \times 10^3$  and  $29.57 \times 10^3 \Omega \cdot cm^2$  for Ti-6Al-2Sn-4Zr-2Mo and Ti-6Al-4V, respectively, with less corrosion resistance in that solution. In Figure 5b, the behavior is very similar, where lower values of  $Z_n$  (see Table 3) are presented by alloys anodized in KOH and a change in slope at middle frequencies relating to the dissolution process. The better properties against corrosion of Ti-6Al-2Sn-4Zr-2Mo are for the different reducing phases. In addition, the presence of Zr composes a better oxide layer [61]. Casanova et al. [62] reported the excellent corrosion resistance of coatings with low porosity in acid solutions. It is seen for Ti-6Al-2Sn-4Zr-2Mo. The presence of Zr helps to reduce the reaction of simple  $TiO_2$  in acid media, where the dissolution of pure titanium depends directly on  $Ti^{3+}$  and the reduction of  $H^+$  to  $H_2$ .

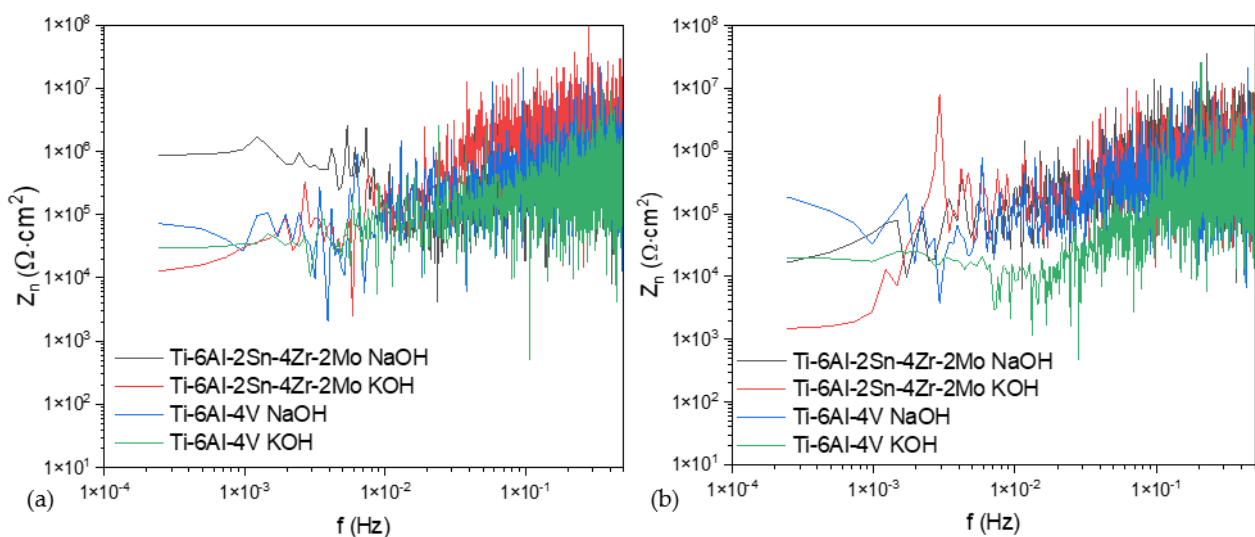


**Figure 5.** Noise impedance ( $Z_n$ ) for Ti-6Al-2Sn-4Zr-2Mo and Ti-6Al-4V alloys anodized and immersed in (a) NaCl and (b)  $H_2SO_4$  at 3.5 wt.%.

### 3.3.2. Wavelets Analysis

Wavelets help to determine the corrosion process that qualitatively occurs on the surface in a wavelet analysis, where the first three crystals are related to metastable pitting, crystals 4 and 6 are related to the localized process, and the last crystal has a uniform process [63,64]. The following equation calculates the energy fraction:

$$ED_j^d = \frac{1}{E} \sum_{n=1}^N d_{j,n}^2 ED_j^s = \frac{1}{E} \sum_{n=1}^N s_{j,n}^2 \quad (3)$$

Figure 6 shows the energy dispersion plot in anodized exposed NaCl (a) and  $H_2SO_4$  (b). Figure 6a shows that Ti-6Al-4V anodized in KOH presented energy accumulation in the first and middle crystals due to the localized process occurring on the surface due to a non-homogenous surface. The rest of the results predominated over a controlled process with low energy accumulation. That controlled process is associated with the accumulation

of corrosion products on the surface, mainly with the system in Figure 6b. In addition, degradation by  $H^+$  absorption can occur. The high energy at the last crystals of anodizing is bigger for the anodized on KOH (except for Ti-6Al-4V anodized on KOH exposed in NaCl), and it is related to a high number of porosities in the system that accumulate the corrosion beginning at a long-time process.

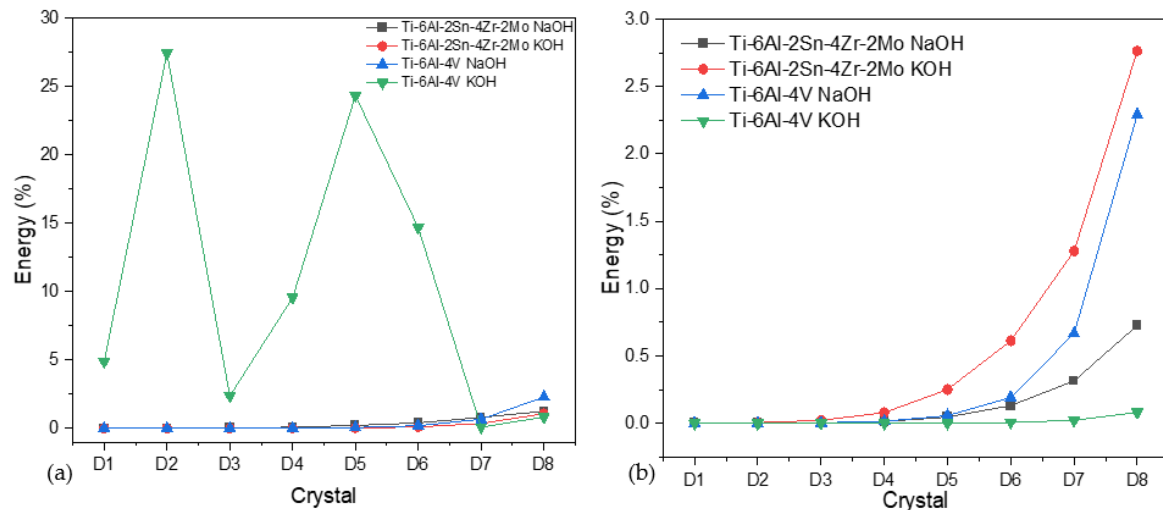


**Figure 6.** Energy dispersion plot (EDP) for Ti-6Al-2Sn-4Zr-2Mo and Ti-6Al-4V alloys anodized and immersed in 3.5 wt.% (a) NaCl and (b) H<sub>2</sub>SO<sub>4</sub> solutions.

The low energy is related to passive systems, as is presented in Figure 6a for all samples except Ti-6Al-4V anodized in KOH and Figure 6b for all samples. Authors such as Carmona-Hernandez et al. [65] suggest that the discontinuous process is like metastable pitting, relating that with this project, the different process is caused by a non-homogenous surface that induces the accumulation of energy in the first crystals of Ti-6Al-4V anodized in KOH. The TiO<sub>2</sub> generated on the surface was stable enough for the rest of the samples, and the nucleation of the localized process did not occur in this experiment's parameters. However, when metastable pitting occurs, it is vital to mention that this is part of the passivation-passivation process; passivation cannot occur without the process of metastable pitting [66]. Therefore, all samples with passivation behavior presented low energy in the first crystals. It is normal to see an equal energy distribution in the first crystals of passivation samples, but the energy is low.

The high energy accumulated in the middle crystals of Ti-6Al-4V anodized in KOH can also be related to an increasing exposition area due to the number of porosities. If the sample has more porosities, the number of reactions increases. However, the heterogeneity of anodized aluminum causes the reactions to occur in specific zones, indicating that localized processes govern the system.

### 3.4. SEM after Corrosion

Figure 7 shows the SEM figures after the corrosion test. Figure 7a shows the superficial morphology after the corrosion test of Ti-6Al-2Sn-4Zr-2Mo exposed in NaCl; the morphology presented a low dissolution of the first roughness layer as well as Figure 7b when exposed to H<sub>2</sub>SO<sub>4</sub>. However, it is worth mentioning that the dissolution is higher when it is exposed to H<sub>2</sub>SO<sub>4</sub>.

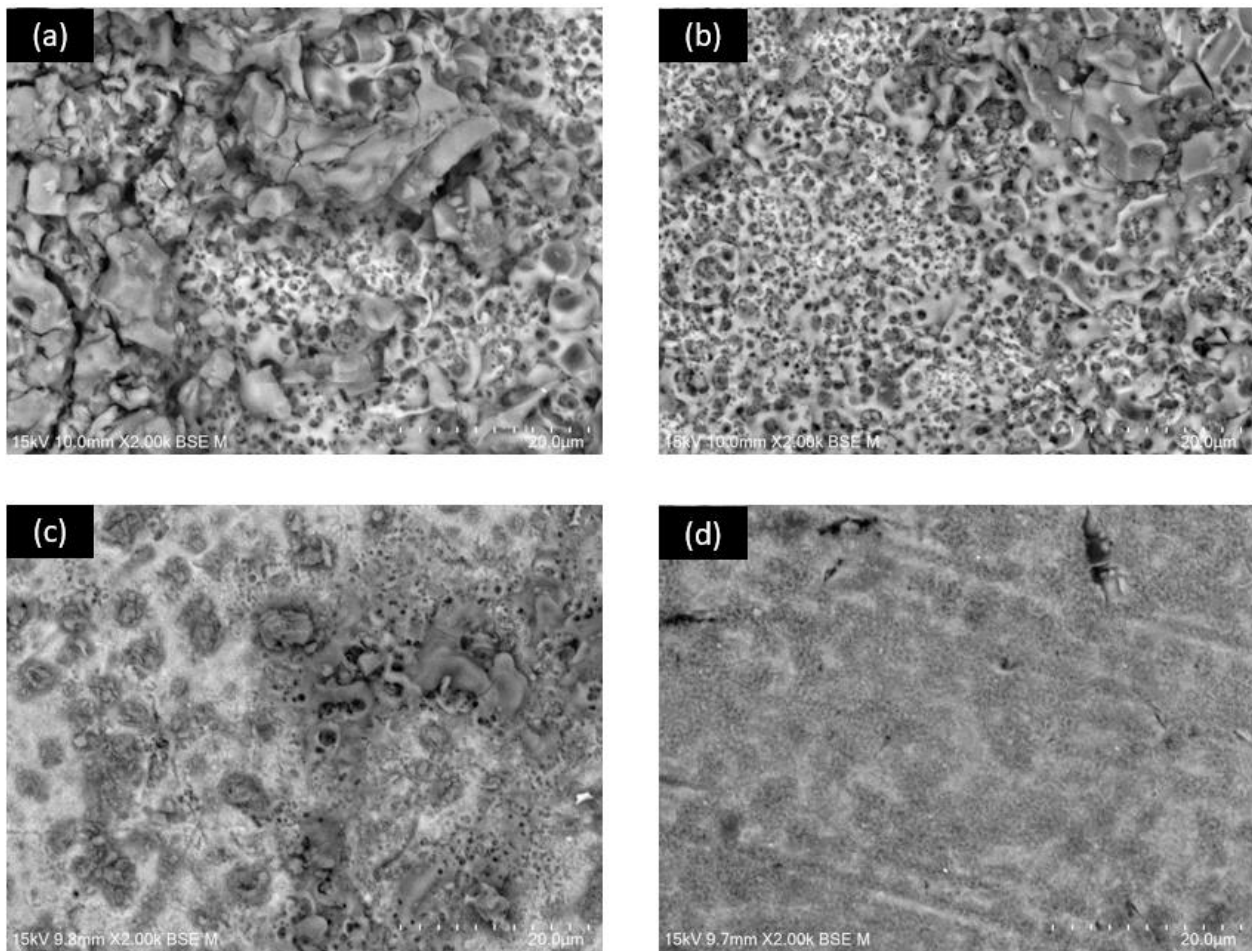


**Figure 7.** SEM-BSE analysis at 2000 $\times$  of Ti-6Al-2Sn-4Zr-2Mo anodized in NaOH exposed in (a) NaCl and (b) H<sub>2</sub>SO<sub>4</sub>. Ti-6Al-2Sn-4Zr-2Mo is anodized in KOH and exposed to (c) NaCl and (d) H<sub>2</sub>SO<sub>4</sub>.

When Ti-6Al-2Sn-4Zr-2Mo is anodized in KOH, the surface changes, indicating that the alloy anodized in this medium is more susceptible to corrosion. Figure 7c shows the behavior when an anodized is exposed to NaCl, and the morphology is different in specific zones; this behavior is related to the non-homogenous nature of the anodized, which makes it susceptible to selective attacks. The same behavior is presented in Figure 7d when exposed to H<sub>2</sub>SO<sub>4</sub>; however, the dissolution was higher, indicating low corrosion resistance.

Figure 8 shows the SEM images of Ti-6Al-4V anodized in NaOH. When the anodized layer was exposed to NaCl, the sample presented a localized corrosion process in the zones with less anodized layers. Figure 8b shows the same morphology, but the localized attack increases, indicating that the heterogeneous anodized metal generates localized corrosion attacks and dissolution in specific areas.

Figure 8c shows the Ti-6Al-4V anodized in KOH when exposed to NaCl, and the anodized material presented localized attack morphology. In Figure 8d, the anodized metal presented a higher dissolution in some zones with pitting, indicating a localized corrosion process in the zones where the anodized metal was weak. The heterogeneous surface of anodized aluminum was an important factor in the localized corrosion processes on the anodized surface of all the alloys.



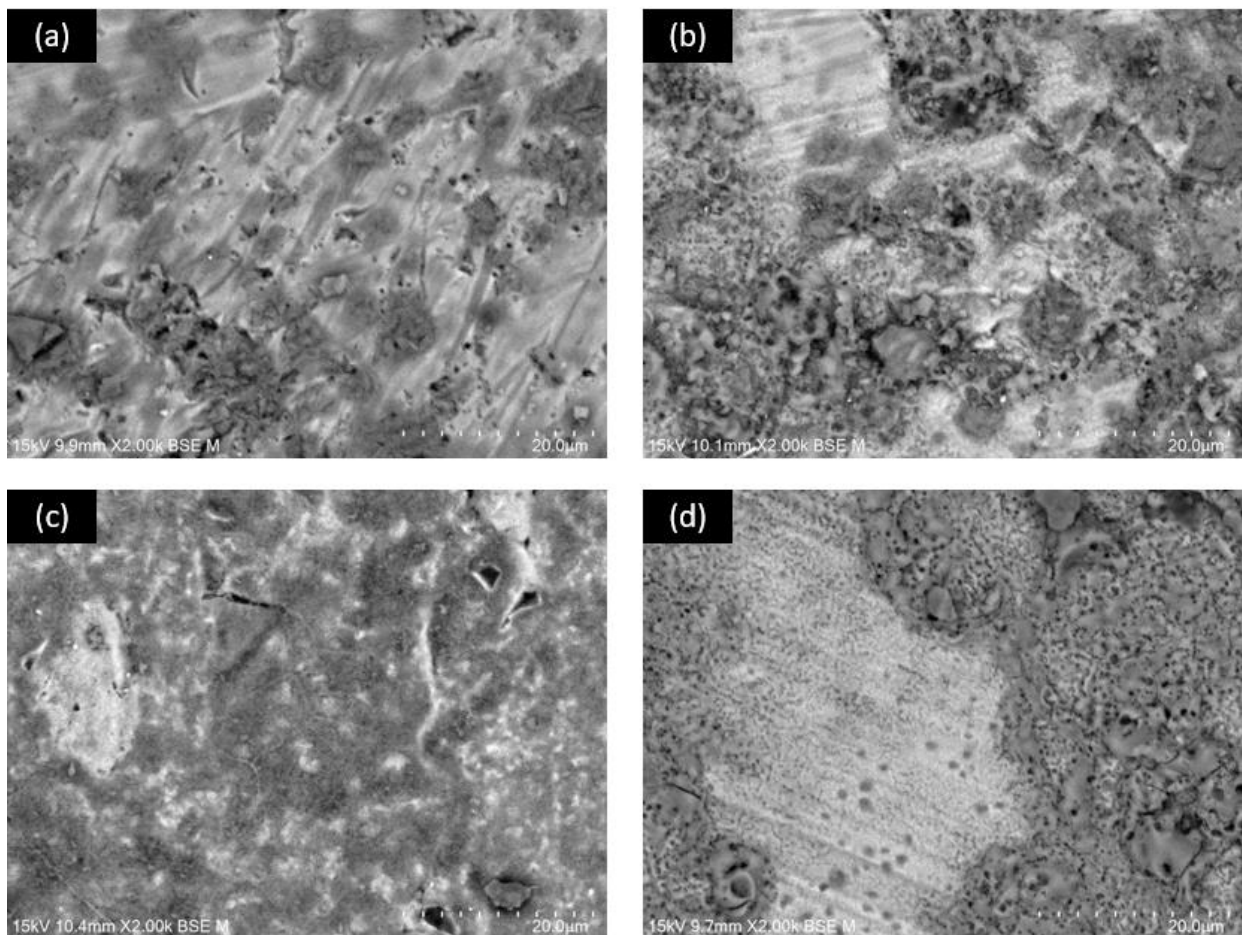


**Figure 8.** SEM-BSE analysis at 2000 $\times$  of Ti-6Al-4V anodized in NaOH exposed in (a) NaCl and (b) H<sub>2</sub>SO<sub>4</sub>. Ti-6Al-4V is anodized in KOH and exposed to (c) NaCl and (d) H<sub>2</sub>SO<sub>4</sub>.

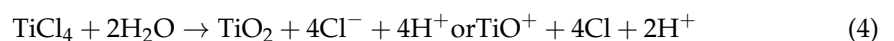
#### 4. Discussion

The behavior of surface morphology is related to an amorphous layer created when electrolytes penetrate cavities during a localized process, creating the growth of an oxide layer in preferential zones [67]. This behavior is associated with the non-homogeneous anodization realized due to Na<sup>+</sup> and K<sup>+</sup> ions deposited in some zones, making the oxide layer grow in preferential zones.

Factors such as the current application are vital to anodized morphology; some authors [68,69] reported that the porosity and the pore size increase with the anodized thickness and the current density applied. In addition, it is important to consider that the time it takes to anodize is related to the number of cracks in the coating. When anodizing time increases, the cracks will propagate through all the interfaces and pores. For that reason, the anodized aluminum presented more cracks. However, using basic media made generating a homogenous oxide layer difficult.

Diverse authors have employed the use of basic electrolytes as anodized media, and they reported a heterogeneous surface [69,70]. Hsu et al. [71] performed research where the creation of porosities is attributed to the penetration of Na<sup>+</sup> and OH<sup>-</sup> ions, provoking a porous barrier of sodium titanate and hydrogen (Na<sub>x</sub>H<sub>2</sub>Ti<sub>3</sub>O<sub>3</sub>) after NaOH exposition. The deposition of Na<sup>+</sup>, K<sup>+</sup>, and OH<sup>-</sup> ions occurs due to surface heterogeneity. When porosity increases, the penetration of those ions increases. It can be related to the localized processes in zones of high energy, such as cracks, porosity, changes in areas, etc. [72,73]. With K, some similarities occur because K and Na are from the same group, presenting the same oxidation and valence numbers.

The values obtained by CPP showed an increase in the current density ( $i_{\text{corr}}$ ) in the Ti-6Al-4V anodized in KOH, which suggests that the process of oxygen and chloride evolution occurs on the surface, affecting the resistance of the anodized. However, the Ti-6Al-2Sn-4Zr-2Mo anodized in both media presented lower values of  $i_{\text{corr}}$ , which occurs due to the presence of Mo, which inhibits the adsorption of  $\text{Cl}^-$  ions, decreasing the dissolution process of the system [74]. On the other hand, when samples have the presence of V, corrosion resistance decreases, as can be observed in the samples anodized with Ti-6Al-4V when CPP presented higher values of  $i_{\text{corr}}$  in comparison to the Ti-6Al-2Sn-4Zr-2Mo. The titanium anodized has a specific behavior when it is exposed to Cl: the water is transported to the pit generated, while the  $\text{TiO}_2$  and  $\text{H}^+$  ions are transported out of the anodized, indicating a dissolution. Moreover, the  $\text{H}^+$  ions penetrate the surface, making it susceptible to breaks caused by the transport of the  $\text{Cl}^-$  and localized attacks in some zones of anodized [75].



Song et al. [17] reported that Ti-alloys with V exposed in saline media presented lower corrosion resistance values, being susceptible to  $\text{Cl}^-$  ions; in CPP curves, the value of passivation range is lower for Ti-6Al-4V than for Ti-6Al-2Sn-4Zr-2Mo; the results of EN presented the same behavior.

All the anodized aluminum exposed to  $\text{H}_2\text{SO}_4$  presented higher corrosion values, even in CPP and EN techniques. It occurred because the  $\text{H}^+$  and  $\text{OH}^-$  are smaller than the  $\text{Na}^+$  and  $\text{Cl}^-$ , creating hydrogen reactions. Therefore, the  $\text{H}_2\text{SO}_4$  electrolyte creates instability on the surface, attacking the porosities and generating anodic reactions. Moreover, the cracks help  $\text{OH}^-$ ,  $\text{SO}_2$ , and  $\text{SO}_4^-$ , according to sulfur degradation [76,77]. For that reason, the corrosion kinetics increase in the  $\text{H}_2\text{SO}_4$  electrolyte.

Also, the Ti-alloys are susceptible to attacks of  $\text{H}^+$  ions, known as hydrogen-induced cracking (HIC). To cause HIC, the surface must absorb hydrogen at the interface of metal/oxide, which causes embrittlement [78]. In this research, hydrogen in the  $\text{H}_2\text{SO}_4$  electrolyte generates  $\text{H}^+$  ions that can sensitize the anodizing, provoking a faster dissolution. For that reason, some parts of the anodized surface cracked and dissolved, facilitating the attack on the surface [79–82]. That behavior is observed when an anodized surface is exposed to NaCl; the  $\text{Cl}^-$  helps to attack the surface after  $\text{H}^+$  breaks the oxide layer.

In future research, complementing electrochemical impedance spectroscopy studies with SEM-EDS of transversal zones, XPS, and XRD is necessary.

## 5. Conclusions

- Results indicated that the titanium alloys anodized on NaOH presented better electrochemical behavior against corrosion. In both techniques, the anodized alloys showed the best behavior.
- The anodized NaOH presented a high passivity range and a minor passivation current, which means a more stable anodized in this medium. The Ti-6Al-2Sn-4Zr-2Mo presented 1.27 V of passivation range.
- The Ti-6Al-2Sn-4Zr-2Mo anodized in NaOH presented the lowest values of  $i_{\text{pass}}$  even in NaCl and  $\text{H}_2\text{SO}_4$ , with values of  $3.03 \times 10^{-6}$  and  $1.67 \times 10^{-7}$  A/cm<sup>2</sup>.
- The decrease in  $i_{\text{pass}}$  for Ti-6Al-2Sn-4Zr-2Mo anodized in KOH exposed to  $\text{H}_2\text{SO}_4$  is related to the formation of an oxide layer at the surface that protects the anodized.
- The alloy Ti-6Al-2Sn-4Zr-2Mo presented better properties when anodized; this behavior is related to the predominance of the  $\alpha$  phase.
- The analysis by power spectral density showed that in a chloride system, the anodized material presented more susceptibility to being attacked by localized processes due to the interstitial role of  $\text{Cl}^-$ .
- The alloy Ti-6Al-4V presented a more heterogeneous surface according to both techniques in CPP, with a lower passivity range and a high current passivation demand ( $2.28 \times 10^{-5}$  A/cm<sup>2</sup>). In PSD and Zn, an abrupt slope change was presented.



- Both techniques contribute to characterizing anodized surfaces and, therefore, to both methods' ability to corroborate information. In electrochemical noise, PSD and wavelets are required to match results due to the complexity of signals (chaotic systems).

**Author Contributions:** Conceptualization, F.A.-C., J.M.J.-M. and C.G.T.; methodology, J.M.J.-M., D.N.-M., A.L.-M., J.C.-M. and L.D.L.-L.; data curation, F.A.-C., J.M.J.-M., J.O.-C., F.E.-L., E.M.-B. and D.N.-M.; formal analysis, C.G.T., L.D.L.-L., F.A.-C. and J.M.J.-M.; writing—review and editing, F.A.-C., J.M.J.-M. and C.G.T. All authors have read and agreed to the published version of the manuscript.

**Funding:** This research was funded by the Universidad Autónoma de Nuevo León (UANL).

**Data Availability Statement:** Not applicable.

**Acknowledgments:** The authors acknowledge the Academic Body UANL—CA-316 “Deterioration and integrity of composite materials”.

**Conflicts of Interest:** The authors declare no conflict of interest.

## References

1. Gialanella, S.; Malandrucolo, A. *Aerospace Alloys*. In *Topics in Mining, Metallurgy and Materials Engineering*; Springer International Publishing: Cham, Switzerland, 2020; ISBN 9783030244392.
2. Mouritz, A.P. *Introduction to Aerospace Materials*; Elsevier: Amsterdam, The Netherlands, 2012; ISBN 9781855739468.
3. Veiga, C.; Davim, J.P.; Loureiro, A.J.R. Properties and Applications of Titanium Alloys: A Brief Review. *Rev. Adv. Mater. Sci.* **2012**, *32*, 133–148.
4. Peters, M.; Kumpfert, J.; Ward, C.H.; Leyens, C. Titanium Alloys for Aerospace Applications. *Adv. Eng. Mater.* **2003**, *5*, 419–427. [[CrossRef](#)]
5. Donachie, M.J. *Titanium—A Technical Guide*; ASM International: The Netherlands, 2000; Volume 55, ISBN 978-0-87170-686-7.
6. Zhang, L.C.; Chen, L.Y. A Review on Biomedical Titanium Alloys: Recent Progress and Prospect. *Adv. Eng. Mater.* **2019**, *21*, 1801215. [[CrossRef](#)]
7. Giriga, S.; Mudali, U.K.; Raju, V.R.; Raj, B. Electrochemical Noise Technique for Corrosion Assessment—A Review. *Corros. Rev.* **2005**, *23*, 107–170. [[CrossRef](#)]
8. Pathania, A.; Kumar, S.A.; Nagesha, B.K.; Barad, S.; Suresh, T.N. Reclamation of Titanium Alloy Based Aerospace Parts Using Laser Based Metal Deposition Methodology. *Mater. Today Proc.* **2021**, *45*, 4886–4892. [[CrossRef](#)]
9. Du, X.Q.; Yang, Q.S.; Chen, Y.; Yang, Y.; Zhang, Z. Galvanic Corrosion Behavior of Copper/Titanium Galvanic Couple in Artificial Seawater. *Trans. Nonferrous Met. Soc. China* **2014**, *24*, 570–581. [[CrossRef](#)]
10. Jáquez-Muñoz, J.M.; Gaona-Tiburcio, C.; Cabral-Miramontes, J.; Nieves-Mendoza, D.; Maldonado-Bandala, E.; Olguín-Coca, J.; López-Léon, L.D.; De Los Rios, J.P.F.; Almeraya-Calderón, F. Electrochemical Noise Analysis of the Corrosion of Titanium Alloys in NaCl and H<sub>2</sub>SO<sub>4</sub> Solutions. *Metals* **2021**, *11*, 105. [[CrossRef](#)]
11. Regonini, D.; Bowen, C.R.; Jaroenworoluck, A.; Stevens, R. A Review of Growth Mechanism, Structure and Crystallinity of Anodized TiO<sub>2</sub> Nanotubes. *Mater. Sci. Eng. R Rep.* **2013**, *74*, 377–406. [[CrossRef](#)]
12. Jaroenworoluck, A.; Regonini, D.; Bowen, C.R.; Stevens, R.; Allsopp, D. Macro, Micro and Nanostructure of TiO<sub>2</sub> Anodised Films Prepared in a Fluorine-Containing Electrolyte. *J. Mater. Sci.* **2007**, *42*, 6729–6734. [[CrossRef](#)]
13. Bocchetta, P.; Chen, L.-Y.; Tardelli, J.D.C.; dos Reis, A.C.; Almeraya-Calderón, F.; Leo, P. Passive Layers and Corrosion Resistance of Biomedical Ti-6Al-4V and β-Ti Alloys. *Coatings* **2021**, *11*, 487. [[CrossRef](#)]
14. Alam, M.J.; Cameron, D.C. Preparation and Characterization of TiO<sub>2</sub> Thin Films by Sol-Gel Method. *J. Sol-Gel Sci. Technol.* **2002**, *25*, 137–145. [[CrossRef](#)]
15. Alharbi, H.F.; Bahri, Y.A.; Sherif, E.-S.M. Influence of Zirconium on the Corrosion Passivation of Titanium in Simulated Body Fluid. *Crystals* **2021**, *11*, 1391. [[CrossRef](#)]
16. Qin, P.; Chen, L.Y.; Liu, Y.J.; Jia, Z.; Liang, S.X.; Zhao, C.H.; Sun, H.; Zhang, L.C. Corrosion and Passivation Behavior of Laser Powder Bed Fusion Produced Ti-6Al-4V in Static/Dynamic NaCl Solutions with Different Concentrations. *Corros. Sci.* **2021**, *191*, 109728. [[CrossRef](#)]
17. Song, H.J.; Kim, M.K.; Jung, G.C.; Vang, M.S.; Park, Y.J. The Effects of Spark Anodizing Treatment of Pure Titanium Metals and Titanium Alloys on Corrosion Characteristics. *Surf. Coat. Technol.* **2007**, *201*, 8738–8745. [[CrossRef](#)]
18. Xia, D.H.; Qin, Z.; Song, S.; Macdonald, D.; Luo, J.L. Combating Marine Corrosion on Engineered Oxide Surface by Repelling, Blocking and Capturing Cl<sup>-</sup>: A Mini Review. *Corros. Commun.* **2021**, *2*, 1–7. [[CrossRef](#)]
19. Jáquez-Muñoz, J.M.; Gaona-Tiburcio, C.; Méndez-Ramírez, C.T.; Baltazar-Zamora, M.Á.; Estupinán-López, F.; Bautista-Margulis, R.G.; Cuevas-Rodríguez, J.; los Rios, J.P.F.-D.; Almeraya-Calderón, F. Corrosion of Titanium Alloys Anodized Using Electrochemical Techniques. *Metals* **2023**, *13*, 476. [[CrossRef](#)]

20. Estupinán-López, F.; Orquiz-Muela, C.; Gaona-Tiburcio, C.; Cabral-Miramontes, J.; Bautista-Margulis, R.G.; Nieves-Mendoza, D.; Maldonado-Bandala, E.; Almeraya-Calderón, F.; Lopes, A.J. Oxidation Kinetics of Ti-6Al-4V Alloys by Conventional and Electron Beam Additive Manufacturing. *Materials* **2023**, *16*, 1187. [[CrossRef](#)]
21. Dziewoński, P.M.; Grzeszczuk, M. Deposition of Thin TiO<sub>2</sub> Layers on Platinum by Means of Cyclic Voltammetry of Selected Complex Ti(IV) Media Leading to Anatase. *Electrochim. Acta* **2009**, *54*, 4045–4055. [[CrossRef](#)]
22. Löbl, P.; Huppertz, M.; Mergel, D. Nucleation and Growth in TiO<sub>2</sub> Films Prepared by Sputtering and Evaporation. *Thin Solid Film.* **1994**, *251*, 72–79. [[CrossRef](#)]
23. Li, X.; Li, C.; Gong, T.; Su, J.; Zhang, W.; Song, Y.; Zhu, X. Comparative Study on the Anodizing Process of Ti and Zr and Oxide Morphology. *Ceram. Int.* **2021**, *47*, 23332–23337. [[CrossRef](#)]
24. Benea, L.; Celis, J.P. Reactivity of Porous Titanium Oxide Film and Chitosan Layer Electrochemically Formed on Ti-6Al-4V Alloy in Biological Solution. *Surf. Coat. Technol.* **2018**, *354*, 145–152. [[CrossRef](#)]
25. İzmir, M.; Ercan, B. Anodization of Titanium Alloys for Orthopedic Applications. *Front. Chem. Sci. Eng.* **2019**, *13*, 28–45. [[CrossRef](#)]
26. Orazem, M.E.; Tribollet, B. Constant-Phase Elements. In *Electrochemical Impedance Spectroscopy*; John Wiley & Sons, Inc.: Hoboken, NJ, USA, 2017; pp. 395–419.
27. Schultze, J.W.; Lohrengel, M.M.; Ross, D. Nucleation and Growth of Anodic Oxide Films. *Electrochim. Acta* **1983**, *28*, 973–984. [[CrossRef](#)]
28. Seçkin, E.; Ürgen, M. A Kinetic Model for Determining Morphology Transitions and Growth Kinetics of Titania Nanotubes during Anodization of Titanium in Ethylene Glycol Based Electrolytes. *Surf. Coat. Technol.* **2021**, *409*, 126840. [[CrossRef](#)]
29. Nakajima, M.; Miura, Y.; Fushimi, K.; Habazaki, H. Spark Anodizing Behaviour of Titanium and Its Alloys in Alkaline Aluminate Electrolyte. *Corros. Sci.* **2009**, *51*, 1534–1539. [[CrossRef](#)]
30. Acevedo-Peña, P.; Vázquez-Arenas, J.G.; Cabrera-Sierra, R.; Lartundo-Rojas, L.; González, I. Hydration and Structural Transformations during Titanium Anodization under Alkaline Conditions. *ECS Trans.* **2013**, *50*, 21–32. [[CrossRef](#)]
31. Uzal, H.; Döner, A. Corrosion Behavior of Titanium Dioxide Nanotubes in Alkaline Solution. *Prot. Met. Phys. Chem. Surf.* **2020**, *56*, 311–319. [[CrossRef](#)]
32. Attabi, S.; Mokhtari, M.; Taibi, Y.; Abdel-Rahman, I.; Hafez, B.; Elmsellem, H. Electrochemical and Tribological Behavior of Surface-Treated Titanium Alloy Ti-6Al-4V. *J. Bio-Tribo-Corros.* **2019**, *5*, 1–11. [[CrossRef](#)]
33. Ormellese, M.; Prando, D.; Nicolis, D.; Bolzoni, F.; Pedferri, M.P. Chemical Oxidation as Repairing Technique to Restore Corrosion Resistance on Damaged Anodized Titanium. *Surf. Coat. Technol.* **2019**, *364*, 225–230. [[CrossRef](#)]
34. Martínez-Aparicio, B.; Martínez-Bastidas, D.; Gaona-Tiburcio, C.; Martin, U.; Cabral-Miramontes, J.; Almeraya-Calderón, F. Localized corrosion of 15–5 PH and 17–4 PH stainless steel in NaCl solution. *J. Solid State Electrochem.* **2023**. [[CrossRef](#)]
35. Jaquez-Muñoz, J.; Gaona-Tiburcio, C.; Lira-Martinez, A.; Zambrano-Robledo, P.; Maldonado-Bandala, E.; Samaniego-Gamez, O.; Nieves-Mendoza, D.; Olguin-Coca, J.; Estupinán-Lopez, F.; Almeraya-Calderon, F. Susceptibility to Pitting Corrosion of Ti-CP2, Ti-6Al-2Sn-4Zr-2Mo, and Ti-6Al-4V Alloys for Aeronautical Applications. *Metals* **2021**, *11*, 1002. [[CrossRef](#)]
36. SAE. *Anodic Treatment of Titanium and Titanium Alloys Solution PH 12.4 Maximum*; SAE: Warrendale, PA, USA, 2018; pp. 1–7.
37. ASTM G61-86; Standard Test Method for Conducting Cyclic Potentiodynamic Polarization Measurements for Localized Corrosion Susceptibility of Iron, Nickel or Cobalt Based Alloys. ASTM International: West Conshohocken, PA, USA, 2010.
38. ASTM G5-14; Standard Reference Test Method for Making Potentiodynamic Anodic Polarization. ASTM International: West Conshohocken, PA, USA, 2014.
39. ASTM G199-09; Standard Guide for Electrochemical Noise Measurement. ASTM International: West Conshohocken, PA, USA, 2020.
40. Apaza-Bedoya, K.; Tarce, M.; Benfatti, C.A.M.; Henriques, B.; Mathew, M.T.; Teughels, W.; Souza, J.C.M. Synergistic Interactions between Corrosion and Wear at Titanium-Based Dental Implant Connections: A Scoping Review. *J. Periodontal Res.* **2017**, *52*, 946–954. [[CrossRef](#)] [[PubMed](#)]
41. Loch, J.; Łukaszczyk, A.; Vignal, V.; Krawiec, H. Corrosion Behaviour of Ti<sub>6</sub>Al<sub>4</sub>V and TiMo<sub>10</sub>Zr<sub>4</sub> Alloys in the Ringer’s Solution: Effect of PH and Plastic Strain. *Solid State Phenom.* **2015**, *227*, 435–438. [[CrossRef](#)]
42. Xu, Y.F.; Xiao, Y.F.; Yi, D.Q.; Liu, H.Q.; Wu, L.; Wen, J. Corrosion Behavior of Ti-Nb-Ta-Zr-Fe Alloy for Biomedical Applications in Ringer’s Solution. *Trans. Nonferrous Met. Soc. China* **2015**, *25*, 2556–2563. [[CrossRef](#)]
43. López, M.F.; Jiménez, J.A.; Gutiérrez, A. Corrosion Study of Surface-Modified Vanadium-Free Titanium Alloys. *Electrochim. Acta* **2003**, *48*, 1395–1401. [[CrossRef](#)]
44. Sherif, E.S.M.; Ragab, S.A.; Abdo, H.S. Role of Vanadium Additions on the Corrosion Mitigation of Ti-6Al-XV Alloy in Simulated Body Fluid. *Metals* **2020**, *10*, 903. [[CrossRef](#)]
45. Liu, Y.; Sun, H.; Liao, F.; Li, G.; Zhao, C.; Cui, C.; Mei, J.; Zhao, Y. Bridging Effects of Sulfur Anions at Titanium Oxide and Perovskite Interfaces on Interfacial Defect Passivation and Performance Enhancement of Perovskite Solar Cells. *ACS Omega* **2021**, *6*, 34485–34493. [[CrossRef](#)]
46. Yan, S.; Song, G.L.; Li, Z.; Wang, H.; Zheng, D.; Cao, F.; Horynova, M.; Dargusch, M.S.; Zhou, L. A State-of-the-Art Review on Passivation and Biofouling of Ti and Its Alloys in Marine Environments. *J. Mater. Sci. Technol.* **2018**, *34*, 421–435. [[CrossRef](#)]
47. Cui, W.F.; Dong, Y.Y.; Bao, Y.C.; Qin, G.W. Improved Corrosion Resistance of Dental Ti50Zr Alloy with (TiZr)N Coating in Fluoridated Acidic Artificial Saliva. *Rare Met.* **2021**, *40*, 2927–2936. [[CrossRef](#)]

48. Li, Y.; Wang, Z.; Shao, M.; Zhang, Z.; Wang, C.; Yan, J.; Lu, J.; Zhang, L.; Xie, B.; He, Y.; et al. Characterization and Electrochemical Behavior of a Multilayer-Structured Ti–N Layer Produced by Plasma Nitriding of Electron Beam Melting TC4 Alloy in Hank's Solution. *Vacuum* **2023**, *208*, 111737. [[CrossRef](#)]
49. Mareci, D.; Chelariu, R.; Gordin, D.M.; Ungureanu, G.; Gloriant, T. Comparative Corrosion Study of Ti–Ta Alloys for Dental Applications. *Acta Biomater.* **2009**, *5*, 3625–3639. [[CrossRef](#)] [[PubMed](#)]
50. Liu, B.; Wang, C.; Chen, Y. Surface Determination and Electrochemical Behavior of IrO<sub>2</sub>–RuO<sub>2</sub>–SiO<sub>2</sub> Ternary Oxide Coatings in Oxygen Evolution Reaction Application. *Electrochim. Acta* **2018**, *264*, 350–357. [[CrossRef](#)]
51. Delgado, D.; Minakshi, M.; Kim, D.-J. Electrochemical Impedance Spectroscopy Studies on Hydrogen Evolution from Porous Raney Cobalt in Alkaline Solution. *Int. J. Electrochem. Sci.* **2015**, *10*, 9379–9394. [[CrossRef](#)]
52. Liu, B.; Ma, B.; Chen, Y.; Wang, C. Corrosion Mechanism of Ti/IrO<sub>2</sub>–RuO<sub>2</sub>–SiO<sub>2</sub> Anode for Oxygen Evolution in Sulfuric Acid Solution. *Corros. Sci.* **2020**, *170*, 108662. [[CrossRef](#)]
53. Fekry, A.M. The Influence of Chloride and Sulphate Ions on the Corrosion Behavior of Ti and Ti-6Al-4V Alloy in Oxalic Acid. *Electrochim. Acta* **2009**, *54*, 3480–3489. [[CrossRef](#)]
54. Yan, J.; Shao, M.; Zhou, Z.; Zhang, Z.; Yi, X.; Wang, M.; Wang, C.; Fang, D.; Wang, M.; Xie, B.; et al. Electrochemical Corrosion Behavior of Ti–N–O Modified Layer on the TC4 Titanium Alloy Prepared by Hollow Cathodic Plasma Source Oxy-nitriding. *Metals* **2023**, *13*, 1083. [[CrossRef](#)]
55. Cottis, R.; Turgose, S. *Electrochemical Impedance and Noise*; NACE International: Houston, TX, USA, 1999; p. 153.
56. Eden, D.A.; Rothwell, A.N. *Electrochemical Noise Data: Analysis, Interpretation and Presentation*; NACE International: Houston, TX, USA, 1992; pp. 1–12.
57. Coakley, J.; Vorontsov, V.A.; Littrell, K.C.; Heenan, R.K.; Ohnuma, M.; Jones, N.G.; Dye, D. Nanoprecipitation in a Beta-Titanium Alloy. *J. Alloys Compd.* **2015**, *623*, 146–156. [[CrossRef](#)]
58. Wei, D.B.; Chen, X.H.; Zhang, P.Z.; Ding, F.; Li, F.K.; Yao, Z.J. Plasma Surface Tantalum Alloying on Titanium and Its Corrosion Behavior in Sulfuric Acid and Hydrochloric Acid. *Appl. Surf. Sci.* **2018**, *441*, 448–457. [[CrossRef](#)]
59. Dong, J.; Liu, Z.; Dong, J.; Ariyanti, D.; Niu, Z.; Huang, S.; Zhang, W.; Gao, W. Self-Organized ZnO Nanorods Prepared by Anodization of Zinc in NaOH Electrolyte. *RSC Adv.* **2016**, *6*, 72968–72974. [[CrossRef](#)]
60. Cheng, F.; Xu, Y.; Zhang, J.; Wang, L.; Zhang, H.; Wan, Q.; Li, W.; Wang, L.; Lv, Z. Growing Carbon Nanotubes In-Situ via Chemical Vapor Deposition and Resin Pre-Coating Treatment on Anodized Ti-6Al-4V Titanium Substrates for Stronger Adhesive Bonding with Carbon Fiber Composites. *Surf. Coat. Technol.* **2023**, *457*, 129296. [[CrossRef](#)]
61. Liu, H.; Yang, J.; Zhao, X.; Sheng, Y.; Li, W.; Chang, C.L.; Zhang, Q.; Yu, Z.; Wang, X. Microstructure, Mechanical Properties and Corrosion Behaviors of Biomedical Ti–Zr–Mo–XMn Alloys for Dental Application. *Corros. Sci.* **2019**, *161*, 108195. [[CrossRef](#)]
62. Casanova, L.; La Padula, M.; Pedefferri, M.P.; Diamanti, M.V.; Ormellese, M. An Insight into the Evolution of Corrosion Resistant Coatings on Titanium during Bipolar Plasma Electrolytic Oxidation in Sulfuric Acid. *Electrochim. Acta* **2021**, *379*, 138190. [[CrossRef](#)]
63. Homborg, A.M.; Oonincx, P.J.; Mol, J.M.C. Wavelet Transform Modulus Maxima and Holder Exponents Combined with Transient Detection for the Differentiation of Pitting Corrosion Using Electrochemical Noise. *Corrosion* **2018**, *74*, 1001–1010. [[CrossRef](#)] [[PubMed](#)]
64. Homborg, A.M.; van Westing, E.P.M.; Tinga, T.; Zhang, X.; Oonincx, P.J.; Ferrari, G.M.; de Wit, J.H.W.; Mol, J.M.C. Novel Time–Frequency Characterization of Electrochemical Noise Data in Corrosion Studies Using Hilbert Spectra. *Corros. Sci.* **2013**, *66*, 97–110. [[CrossRef](#)]
65. Carmona-Hernández, A.; Orozco-Cruz, R.; Carpio-Santamaria, F.A.; Campechano-Lira, C.; López-Huerta, F.; Mejía-Sánchez, E.; Contreras, A.; Galván-Martínez, R. Electrochemical Noise Analysis of the X70 Pipeline Steel under Stress Conditions Using Symmetrical and Asymmetrical Electrode Systems. *Metals* **2022**, *12*, 1545. [[CrossRef](#)]
66. Zhang, Z.; Li, X.; Zhao, Z.; Bai, P.; Liu, B.; Tan, J.; Wu, X. In-Situ Monitoring of Pitting Corrosion of Q235 Carbon Steel by Electrochemical Noise: Wavelet and Recurrence Quantification Analysis. *J. Electroanal. Chem.* **2020**, *879*, 114776. [[CrossRef](#)]
67. Mazzarolo, A.; Curioni, M.; Vincenzo, A.; Skeldon, P.; Thompson, G.E. Anodic Growth of Titanium Oxide: Electrochemical Behaviour and Morphological Evolution. *Electrochim. Acta* **2012**, *75*, 288–295. [[CrossRef](#)]
68. Laurindo, C.A.H.; Torres, R.D.; Mali, S.A.; Gilbert, J.L.; Soares, P. Incorporation of Ca and P on Anodized Titanium Surface: Effect of High Current Density. *Mater. Sci. Eng. C* **2014**, *37*, 223–231. [[CrossRef](#)]
69. Zhang, Y.; Fan, H.; Ding, X.; Yan, Q.; Wang, L.; Ma, W. Simulation of Anodizing Current–Time Curves and Morphology Evolution of TiO<sub>2</sub> Nanotubes Anodized in Electrolytes with Different NH<sub>4</sub>F Concentrations. *Electrochim. Acta* **2015**, *176*, 1083–1091. [[CrossRef](#)]
70. Burleigh, T.D.; Dotson, T.C.; Dotson, K.T.; Gabay, S.J.; Sloan, T.B.; Ferrell, S.G. Anodizing Steel in KOH and NaOH Solutions. *J. Electrochem. Soc.* **2007**, *154*, C579. [[CrossRef](#)]
71. Hsu, H.C.; Hsu, S.K.; Wu, S.C.; Hung, Y.H.; Ho, W.F. Surface Modification of Nanotubular Anodized Ti–7.5Mo Alloy Using NaOH Treatment for Biomedical Application. *Thin Solid Film.* **2020**, *710*, 138273. [[CrossRef](#)]
72. Yamaguchi, S.; Takadama, H.; Matsushita, T.; Nakamura, T.; Kokubo, T. Preparation of Bioactive Ti–15Zr–4Nb–4Ta Alloy from HCl and Heat Treatments after an NaOH Treatment. *J. Biomed. Mater. Res. Part A* **2011**, *97A*, 135–144. [[CrossRef](#)] [[PubMed](#)]
73. Hsu, H.-C.; Wu, S.-C.; Hsu, S.-K.; Chuang, S.-H.; Ho, W.-F. Surface Modification of Commercially Pure Ti Treated with Aqueous NaOH Treatment and Ethyl Alcohol Aging. *J. Med. Biol. Eng.* **2013**, *33*, 331–336. [[CrossRef](#)]

74. Martinez, A.L.; Flamini, D.O.; Saidman, S.B. Corrosion Resistance Improvement of Ti-6Al-4V Alloy by Anodization in the Presence of Inhibitor Ions. *Trans. Nonferrous Met. Soc. China (Engl. Ed.)* **2022**, *32*, 1896–1909. [[CrossRef](#)]
75. Prando, D.; Nicolis, D.; Pedferri, M.P.; Ormellese, M. Pitting Corrosion on Anodized Titanium: Effect of Halides. *Mater. Corros.* **2018**, *69*, 1441–1446. [[CrossRef](#)]
76. Córdoba-Torres, P. Relationship between Constant-Phase Element (CPE) Parameters and Physical Properties of Films with a Distributed Resistivity. *Electrochim. Acta* **2017**, *225*, 592–604. [[CrossRef](#)]
77. Rajan, S.T.; Anusha, T.V.V.; Terada-Nakaishi, M.; Chen, P.; Hanawa, T.; Nandakumar, A.K.; Subramanian, B. Zirconium-Based Metallic Glass and Zirconia Coatings to Inhibit Bone Formation on Titanium. *Biomed. Mater.* **2020**, *15*, 065019. [[CrossRef](#)]
78. Prando, D.; Brenna, A.; Diamanti, M.V.; Beretta, S.; Bolzoni, F.; Ormellese, M.; Pedferri, M.P. Corrosion of Titanium: Part 1: Aggressive Environments and Main Forms of Degradation. *J. Appl. Biomater. Funct. Mater.* **2017**, *15*, e291–e302. [[CrossRef](#)]
79. Madina, V.; Azkarate, I. Compatibility of Materials with Hydrogen. Particular Case: Hydrogen Embrittlement of Titanium Alloys. *Int. J. Hydrogen Energy* **2009**, *34*, 5976–5980. [[CrossRef](#)]
80. Shoesmith, D.W.; Noël, J.J.; Hardie, D.; Ikeda, B.M. Hydrogen Absorption and the Lifetime Performance of Titanium Nuclear Waste Containers. *Corros. Rev.* **2000**, *18*, 331–359. [[CrossRef](#)]
81. Hua, F.; Mon, K.; Pasupathi, P.; Gordon, G.; Shoesmith, D. Modeling the Hydrogen-Induced Cracking of Titanium Alloys in Nuclear Waste Repository Environments. *JOM* **2005**, *57*, 20–26. [[CrossRef](#)]
82. Christ, H.J.; Senemmar, A.; Decker, M.; Prüßner, K. Effect of Hydrogen on Mechanical Properties of  $\beta$ -Titanium Alloys. *Sadhana* **2003**, *28*, 453–465. [[CrossRef](#)]

**Disclaimer/Publisher’s Note:** The statements, opinions and data contained in all publications are solely those of the individual author(s) and contributor(s) and not of MDPI and/or the editor(s). MDPI and/or the editor(s) disclaim responsibility for any injury to people or property resulting from any ideas, methods, instructions or products referred to in the content.